ON THE DEVELOPMENT OF FINITE VOLUME METHODS FOR COMPUTATIONAL SOLID MECHANICS

Alejandro C. Limache[a] and Sergio R. Idelsohn[b]

[a]*International Center of Computational Methods in Engineering (CIMEC)*
CONICET-INTEC, Santa Fe, Argentina, alejandrolimache@hotmail.com,
http://www.cimec.org.ar/alimache
[b]*CIMNE, Universidad Politécnica de Cataluña, Barcelona, España*

Keywords: Finite Volume method, Finite Element method, Finite Deformations, Piola-Kirchhoff Stress Tensor, Objectivity

Abstract. Since its initial development as a tool for structural analysis around the mid-fifties the Finite Element Method (FEM) has evolved to become the most popular and used method in modern Computational Solid Mechanics. On the other hand, the Finite Volume Method (FVM) born almost at the same time, has evolved too and become one of the most popular methods in the area of Computational Fluid Mechanics. Both methods have surpassed the historical finite differences method and other discretization methods, and nowadays, researchers typically use one or the other to obtain numerical simulations of all types of physical phenomena. However, although FEM is at present being actively used to solve the equations of compressible and incompressible flows, there are not many works about the usage of FVM in solving the equations of solid materials. The physical flavor, the conservation properties and some properties of reduced integration of the FVM, are advantages that could be very useful in the context of Computational Solid Mechanics as they are in the context of Computational Fluid Mechanics (CFD). In the present work we show our first results in our attempt to develop a Finite Volume Method for Non-linear Solid Mechanics.

1   INTRODUCTION

Since its initial development as a tool for structural analysis around the mid-fifties the Finite Element Method (FEM) (Zienkiewicz and Taylor (1991), Cook et al. (2001), Hughes (2000)) has evolved to become the most popular and used method in modern Computational Solid Mechanics (ABAQUS (2007), Szabo and Babuska (1991), Ramesh and Maniatty (2005)). On the other hand, the Finite Volume Method (FVM) (Leveque (2002), Versteeg and Malalasekera (1995)) born almost at the same time, has evolved too and become one of the most popular methods in the area of Computational Fluid Mechanics (CFX (2007), Hubbard and Roe (2000), Frink and Pirzadeh (1998), Biedron (2005)). Both methods have surpassed the historical finite differences method and other discretization methods, and nowadays, researchers typically use one or the other to obtain numerical simulations of all types of physical phenomena.

Nowadays, the popularity of FEM has also extended over the domain of Computational Fluid Mechanics and it is used for the simulation of compressible and incompressible flows (PETScFEM (2007), FEATFLOW (2007), Matallah et al. (1998), Souli et al. (2000)),. However, the converse is not true, there are comparatively not many works describing the usage of FVM in structural or solid mechanics. There is not a clear explanation for this situation, but one could argue it may be due to the two following reasons. First, FEM has an already builded mathematical background that more easily allows to get convergence proofs and to perform error analysis (Johnson (1987)). Second, many fluidicists and solidicists tend to stay into the numerical schemes they have traditionally employed, producing the particular situation where the FVM mainly used by fluidicists has not been explored by solidicists.

The FVM has been so succesful in CFD and its features so interesting that it is a pity that its usage has not been further explored in the context of solid mechanics. However, recently there has been a surge in the interest for the development of CSM programs based on FVM (Chung and Zou (2001), Rente and Oliveira (2000), Taylor et al. (1999b), Wheel (1999), Taylor et al. (1999a), Zarrabi and Basu (2000), Slone et al. (2003), Howell and Ball (2002), Teran et al. (2003), Bijelonja et al. (2006)). This new surge is not surprising if one has in mind the interesting properties that FVM has: 1) FVM has many of the characteristics and virtues of FEM, both are weak/integral formulations and both are independent of the domain geometry, and as a consequence both are superior to finite differences. 2) FVM allows for the strict conservation of physical quantities in the control volume Lax and Wendroff (1960), Leer (1982). 3) FVM has a strong physical and geometric flavor instead of the variational flavor of FEM. 4) FVM seems to be superior to FEM in problems dealing with discontinuities as the cases of shock-capturing Rumsey and Vatsa (1993), Atwood (1992), Cheatwood and Gnoffo (1996) in transonic and supersonic flows. 5) The ability of FVM in shock capturing can be explained in its flexibility to define interpolating functions, allowing for example to introduce state variables that are discontinuos between elements. This virtue could be important in problems dealing with material failure where fisures or fractures can be seen as discontinuities in state variables. 6) FVM, like FEM, can be used not only in problems of computational mechanics but also in other areas of physics and sciences. For example, it can be used to solve Maxwell equations of electromagnetism Chung and Zou (2001). 7) Researchers that have worked on FVM formulations for solids have reported results that are equally comparable or surpass results obtained by FEM (Rente and Oliveira (2000)-Bijelonja et al. (2006)). 8) Other researchers have developed hibrid schemes (FEM-FVM) where FVM is used to compute the internal forces produces by the Cauchy Tensor Chen et al. (2001). They report that these schemes perform better than conventional FEM methods, allowing for example stable nodal integration. Hibrid schemes have been

also used with success for viscoelastic flows Chandio et al. (2004), multi-phase flows Geiger et al. (2003) and shock capturing Bergamaschi et al. (1999). 10) Another key feature of FVM is that internal forces and fluxes are computed by integration in a lower dimension (surfaces) than FEM (volumes). The reduction in dimensionality of a problem, is generally an advantage. Reduced integration could make FVM more exact and faster than FEM.

Under the considerations made in the above paragraphs, at CIMEC, we have started the design of numerical programs based on FVM for Computational Mechanics. The main objective is to develop an alternative method which potentially could be more robust, accurate and faster than FEM. We already have experience with the usage and success of FVM in the context of fluid mechanics Limache and Cliff (2000) and we want to extend this success by developing FVM formulations for CSM. The ultimate idea is to create a monolithic numerical scheme to handle fluid-interaction problems and other multy-physics problems.

In the present work we describe the Finite Volume formulation that we have developed for non-linear solid mechanics. The developed formulation has been implemented and, integrated into the numerical program `MulPhys` Limache (2007). The new FV module is named `MulPhys-FV`. As it will be seen, `MulPhys-FV` can perform simulations dealing with large deformations, large rotations and large displacements.

The paper is ordered as follows. In the next Section, the theoretical formulation necessary for finite-deformations is presented, followed by a description of the Finite Volume scheme in Section 3. In Section 4, the numerical results using the developed program are presented and comparisons are made with the results obtained with `MulPhys-FEM`. MulPhys-FEM is a FEM-based numerical program developed at CIMEC that can be used for the simulation of non-linear solid mechanics with finite-deformations. Finally, we close the paper with a brief discussion of our results and some conclusions.

2 A FRAMEWORK FOR FINITE-DEFORMATIONS

2.1 Reference and Current Configurations

In continuum mechanics, the equations describing the dynamics and motion of material bodies are defined. A material body is formed by a compact set of material particles. We can represent the body by the specification of its geometrical and material properties at a certain moment when the body was available to us for inspection. This specification is called the *reference configuration*, and at such configuration we can assign a one to one correspondence between each particle χ and the vector position $\boldsymbol{X}$ defining the particle's location with respect to the *reference frame* defined at the moment of inspection. At the reference configuration, we know the volume or region Ω^0 occupied by the body and we can get any of its physical properties. These physical properties can be scalar, vector or tensor quantities. For example, we can obtain its density field ρ^0

$$\rho^0 = \bar{\rho}(\boldsymbol{X}) \tag{1}$$

or its stress state field, the Cauchy Stress $\boldsymbol{\sigma}^0$:

$$\boldsymbol{\sigma}^0 = \overline{\boldsymbol{\sigma}}(\boldsymbol{X}) \tag{2}$$

Sometimes it is convenient to choose the reference configuration as a state of zero stress.

To study the kinematics of our material body. Let us assume that at a given time the body is moving, rotating and deforming so its configuration changes as time evolves. We can fully describe the body's change in configuration by tracking the material particles thru its vector

position $\boldsymbol{x}$ in the physical space. In particular, we can account for the configuration changes and perform this tracking by specifying the particles' position $\boldsymbol{x}$ as a function of time and their positions in the reference configuration:

$$\boldsymbol{x} = \overline{\boldsymbol{x}}(\boldsymbol{X}, t) \tag{3}$$

Since t usually represents the current time, the configuration defined by the mapping (3) is usually called *current configuration*. The function $\overline{\boldsymbol{x}}$ is called *deformation map* because it defines the deformation of the body from the reference configuration into the current configuration. In the current configuration the volume occupied by the body will be denoted by Ω and its density field and stress field will be denoted by ρ and $\boldsymbol{\sigma}$, respectively. Note that the corresponding fields in the reference configuration are denoted in the same way but using the upper-index "0".

A measure of the change of configuration is given by the *deformation gradient* tensor:

$$\boldsymbol{F} = \overline{\boldsymbol{F}}(\boldsymbol{X}, t) = \frac{\partial \overline{\boldsymbol{x}}(\boldsymbol{X}, t)}{\partial \boldsymbol{X}} = \frac{\partial \boldsymbol{x}}{\partial \boldsymbol{X}} = \text{Grad}(\overline{\boldsymbol{x}}) \tag{4}$$

Note that $\boldsymbol{F}$ defines how a material differential changes:

$$d\boldsymbol{x} = \boldsymbol{F} \cdot d\boldsymbol{X} = \frac{\partial \boldsymbol{x}}{\partial \boldsymbol{X}} \cdot d\boldsymbol{X} \tag{5}$$

2.2 Strong Form of Equations of Continuum Mechanics

The equations of conservation of mass and momentum define the dynamics, deformation and motion of material bodies. They can be written either in the reference configuration or in the current configuration. Most people, particularly fluidicists, are used to see these equations in the current configuration, they are:

$$\frac{D\rho}{Dt} + \rho \, \text{div}(\boldsymbol{v}) = 0 \tag{6}$$

$$\rho \frac{D\boldsymbol{v}}{Dt} = \text{div}(\boldsymbol{\sigma}) + \rho \boldsymbol{b} \tag{7}$$

where $\frac{D}{Dt}()$ denotes the material time-derivative, div denotes de divergence operator in the current configuration and where $\boldsymbol{b}$ denotes the external body forces per unit of mass. However, in our case, it is most convenient to represent these equations in the reference configuration Gurtin (1981), they are:

$$\rho J = \rho^0 \tag{8}$$

$$\rho^0 \frac{D\boldsymbol{v}}{Dt} = \text{Div}(\boldsymbol{P}) + \rho^0 \boldsymbol{b^0} \tag{9}$$

where J stands for the determinant of the deformation gradient and where $\boldsymbol{P}$ represents the First Piola Kirchhoff Stress Tensor:

$$\boldsymbol{P} = \boldsymbol{\sigma} \cdot J \boldsymbol{F}^{-T} \tag{10}$$

The above equations are complete when the Cauchy stress is linked to a deformation measure thru a constitutive equation. The constitutive equation defines the material characteristics and

here, we will only discuss the case of an hyperelastic material Ottosen and Ristinmaa (2005) whose constitutive equation is given by:

$$\boldsymbol{\sigma} = \boldsymbol{F} \cdot \boldsymbol{C} : \boldsymbol{E} \cdot J^{-1}\boldsymbol{F}^T \tag{11}$$

where $\boldsymbol{C}$ is the fourth order isotropic material tensor and $\boldsymbol{E}$ is the Green Lagrangean Strain Tensor Ogden (1984).

The above system of equations (8)-(11) are fully objective and they let us to describe the dynamics and finite deformations of such hyperelastic material body. In the next section, instead of presenting an stardard FEM-based approach a new Finite Volume formulation will be presented. Furthermore, the developed formulation is general and not limited to small-deformations or linear-elasticity theory Onate (1995).

3 A FINITE VOLUME FORMULATION FOR COMPUTATIONAL SOLID MECHANICS

The FVM, like FEM, is based on a weak form obtained by integration of the differential equations. Although there are some analogies with FEM, the FVM can be simply seen as the conservation form of the differential equations in discrete volumes $V^{(i)}$ around each of the nodes i that define the discretization of the reference volume Ω^0 where the equations are defined. Given any of these discrete volumes $V^{(i)}$ the conservation form of the equation of momentum (9) is given by:

$$\int_{V^{(i)}} \rho^0 \frac{D\boldsymbol{v}}{Dt} dV^{(i)} = \int_{\Gamma^{(i)}} \boldsymbol{P} \cdot \boldsymbol{N} d\Gamma^{(i)} + \int_{V^{(i)}} \rho^0 \boldsymbol{b}^0 dV^{(i)} \tag{12}$$

where $\Gamma^{(i)}$ defines the boundary surface of $V^{(i)}$ and $\boldsymbol{N}$ is the outward-pointing unit normal along the boundary surface $\Gamma^{(i)}$. Note that the above equations can be obtained by a Petrov-Galerking procedure where the weighting functions $w^{(i)}$ are just piecewise constant functions being equal to 1 in $V^{(i)}$ and zero otherwise.

In our case the computational domain Ω^0 is discretized by a delaunay triangularization, the control volumes $V^{(i)}$ are centered in the nodes forming the vertices of the triangles and their boundary $\Gamma^{(i)}$ is formed by connecting the centroids of each triangle to the mid-points of the edges, as shown in figure 1. There, the surface boundary $\Gamma^{(1)}$ is defined through the segments passing by the points $a, b, c, d, e, f, g, h, i, j$. Note that this procedure defines a set of non-overlapping control volumes that completely cover the domain Ω^0. The state variables $\{\boldsymbol{x}, \boldsymbol{v}\}$ that describe the motion and deformation of the body are discretized in terms of their nodal values $\{\hat{\boldsymbol{x}}, \hat{\boldsymbol{v}}\}$ at the nodes (i). With these discrete variables all the remaining physical variables can be computed assuming a piece-wize linear variation similar to the one used in FEM with linear elements.

Note that if a first order discretization in time is used, then if the state $\{\hat{\boldsymbol{x}}^n, \hat{\boldsymbol{v}}^n\}$ is known at time $t = t^n$, the system has to be solved for time $t = t^{n+1}$:

$$\int_{V^{(i)}} \frac{\rho^0}{\triangle t} \boldsymbol{v}^{n+1} dV^{(i)} - \int_{V^{(i)}} \frac{\rho^0}{\triangle t} \boldsymbol{v}^n dV^{(i)} = \int_{\Gamma^{(i)}} \boldsymbol{P}^{n+1} \cdot \boldsymbol{N} d\Gamma^{(i)} + \int_{V^{(i)}} \rho^0 \boldsymbol{b}^0 dV^{(i)} \tag{13}$$

The above equation together with a relationship of the form:
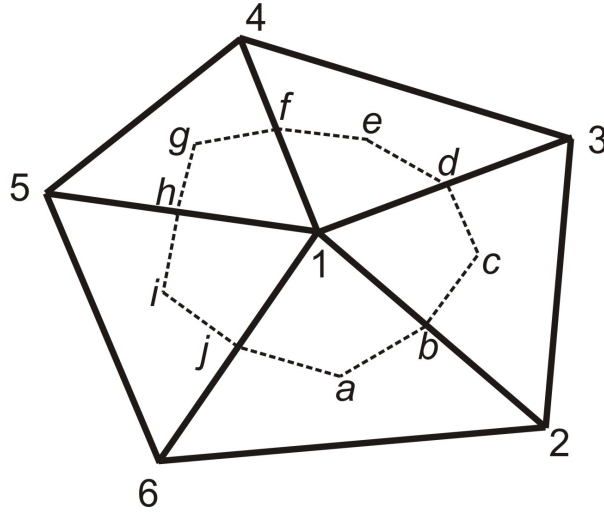
$$\frac{x^{n+1} - x^n}{\triangle t} = v^{n+1} \tag{14}$$

Figure 1: Finite Volume Cells

defines a set of implicit non-linear equations that has to be solved for $\{\hat{\boldsymbol{x}}^{n+1}, \hat{\boldsymbol{v}}^{n+1}\}$.

We briefly discuss how to compute the *mass terms*, i.e. the RHS terms of eq. (13), all other terms in the equation are handled in a similar way. Consider an arbitrary triangle $\triangle_{123}$ obtained using a triangulation of the domain, its vertices correspond to nodes numbered locally by 1, 2 and 3 whose coordinates are denoted by:

$$\{\hat{\boldsymbol{x}}_1 = (x_1, y_1), \hat{\boldsymbol{x}}_2 = (x_2, y_2), \hat{\boldsymbol{x}}_3 = (x_3, y_3)\} \tag{15}$$

The area of the triangle $A^{(e)}$ is given by:

$$A^{(e)} = \frac{1}{2}|J^{(e)}| = \frac{1}{2}\det(J^{(e)}) = \frac{1}{2}[(x_2 - x_1)(y_3 - y_1) - (x_3 - x_1)(y_2 - y_1)] \tag{16}$$

where $J^{(e)}$ is the Jacobian of the transformation of the triangle to a master triangle:

$$J^{(e)} = \left[\begin{array}{cc} x_2 - x_1 & y_2 - y_1 \\ x_3 - x_1 & y_3 - y_1 \end{array} \right]$$

The centroid $\boldsymbol{c}$ of the triangle is the point where its medians (the lines joining each vertex with the midpoint of the opposite side) intersect. Its coordinates are given by:

$$\boldsymbol{c} = \frac{1}{3}(\hat{\boldsymbol{x}}_1 + \hat{\boldsymbol{x}}_2 + \hat{\boldsymbol{x}}_3) \tag{17}$$

The medians divide the triangle in six sub-triangles of equal area that join at the centroid, then if $A^{(e)}$ denotes de area of the triangle, each of this new sub-triangles have areas $\frac{A^{(e)}}{6}$. If the midpoint of the side of the triangle between node i and node j is denoted by $\boldsymbol{m}_{ij}$ we have that:

$$\boldsymbol{m}_{ij} = \frac{1}{2}(\hat{\boldsymbol{x}}_i + \hat{\boldsymbol{x}}_j) \tag{18}$$

Suppose a field v is defined by a linear interpolation in the triangle, so in terms of its nodal values $\{\hat{v}_1, \hat{v}_2, \hat{v}_3\}$ and the corresponding nodal shape functions N_i, v is given by:

$$v(\boldsymbol{x}) = N_1(\boldsymbol{x})\hat{v}_1 + N_2(\boldsymbol{x})\hat{v}_2 + N_3(\boldsymbol{x})\hat{v}_3 \tag{19}$$

From the equivalence between the shape functions and the area coordinates L_i:

$$N_i = L_i \tag{20}$$

we can write equation (19) as:

$$v(\boldsymbol{x}) = v(L_1, L_2, L_3) = L_1(\boldsymbol{x})\widehat{v}_1 + L_2(\boldsymbol{x})\widehat{v}_2 + L_3(\boldsymbol{x})\widehat{v}_3 \tag{21}$$

The area coordinates at the centroid satisfy:

$$L_i(\boldsymbol{c}) = \frac{1}{3} \quad i = 1, 2, 3 \tag{22}$$

Using this in eq. (21) we get that the value of v at the centroid is given by

$$\widehat{v}_{\boldsymbol{c}} = v(\boldsymbol{c}) = \frac{1}{3}(\widehat{v}_1 + \widehat{v}_2 + \widehat{v}_3) \tag{23}$$

Similarly at the midpoints $\boldsymbol{m}_{ij}$ we have:

$$\widehat{v}_{\boldsymbol{m}_{ij}} = v(\boldsymbol{m}_{ij}) = \frac{1}{2}(\widehat{v}_i + \widehat{v}_j) \tag{24}$$

Now let us note that the integral of the field v in the triangle is given by

$$\int_{A^{(e)}} v(\boldsymbol{x})\,\mathrm{da} = \int_0^1 \int_0^{1-L_3} v(L_1, L_2, L_3)\det(J^{(e)})dL_2 dL_3$$

Using numerical integration of the RHS (i.e. in the master triangle) with n_{pg} Gauss-points:

$$\int_{A^{(e)}} v(\boldsymbol{x})\,\mathrm{da} = \sum_{p=1}^{n_{\mathrm{pg}}} v(L_{1_p}, L_{2_p}, L_{3_p})\det(J^{(e)})W_p \tag{25}$$

For linear functions we just need one integration point $n_{\mathrm{pg}} = 1$ where $\boldsymbol{x}_{\mathrm{pg}} = \boldsymbol{c}$ and $W_{\mathrm{pg}} = 1/2$ so:

$$\int_{A^{(e)}} v(\boldsymbol{x})\,\mathrm{da} = v(\boldsymbol{c})2A^{(e)}\frac{1}{2} = \frac{1}{3}(\widehat{v}_1 + \widehat{v}_2 + \widehat{v}_3)A^{(e)} \tag{26}$$

Now consider the portion $V^{(1,e)}$ of the finite-volume cell $V^{(1)}$ around node 1 that belongs to the triangle $\triangle^{(e)}$, see figure 2. From the figure, we have that $V^{(1,e)}$ is formed by the two subtriangles that join at node 1. Then from eq. (26) we have that:

$$\int_{V^{(1,e)}} v(\boldsymbol{x})\,\mathrm{da} = \frac{1}{3}(\widehat{v}_1 + \widehat{v}_{\boldsymbol{m}_{12}} + \widehat{v}_{\boldsymbol{c}})\frac{A^{(e)}}{6} + \frac{1}{3}(\widehat{v}_1 + \widehat{v}_{\boldsymbol{m}_{13}} + \widehat{v}_{\boldsymbol{c}})\frac{A^{(e)}}{6} \tag{27}$$

$$\int_{V^{(1,e)}} v(\boldsymbol{x})\,\mathrm{da} = \frac{1}{3}\frac{A^{(e)}}{6}(2\widehat{v}_1 + \widehat{v}_{\boldsymbol{m}_{12}} + \widehat{v}_{\boldsymbol{m}_{13}} + 2\widehat{v}_{\boldsymbol{c}}) \tag{28}$$

Using eqs. (23) and (24):

$$\int_{V^{(1,e)}} v(\boldsymbol{x})\,\mathrm{da} = \frac{1}{3}\frac{A^{(e)}}{6}(2\widehat{v}_1 + \frac{1}{2}\widehat{v}_1 + \frac{1}{2}\widehat{v}_2 + \frac{1}{2}\widehat{v}_1 + \frac{1}{2}\widehat{v}_3 + \frac{2}{3}\widehat{v}_1 + \frac{2}{3}\widehat{v}_2 + \frac{2}{3}\widehat{v}_3) \tag{29}$$
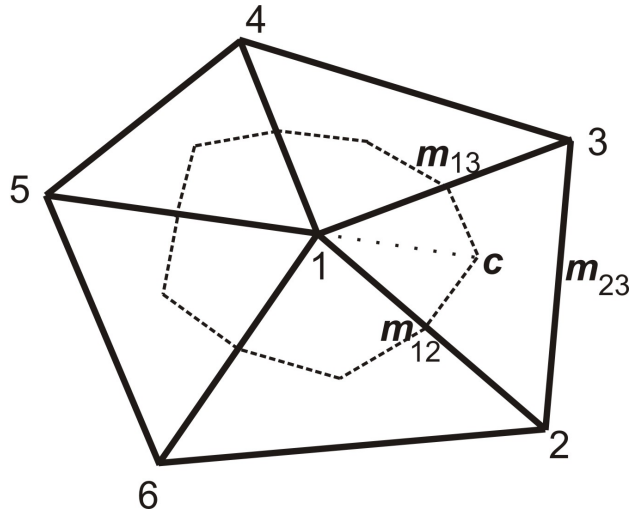
Figure 2: Finite Volume Cells and their triangular components

$$\int_{V^{(1,e)}} v(\boldsymbol{x})\,\mathrm{da} = \frac{1}{3}\frac{A^{(e)}}{6}\left((3+\frac{2}{3})\widehat{v}_1 + (\frac{1}{2}+\frac{2}{3})\widehat{v}_2 + (\frac{1}{2}+\frac{2}{3})\widehat{v}_3\right) \tag{30}$$

$$\int_{V^{(1,e)}} v(\boldsymbol{x})\,\mathrm{da} = \frac{1}{3}\frac{A^{(e)}}{36}(22\widehat{v}_1 + 7\widehat{v}_2 + 7\widehat{v}_3) \tag{31}$$

The above formula defines the elemental contribution to the mass matrix coefficients associated to node 1. From equation (31) it follows that the Finite Volume mass matrix coefficients are different to the mass matrix coefficients produced by a FEM formulation Zienkiewicz and Taylor (1991).

The described discretization leads to a system of non-linear equations for time $t = t^{n+1}$, that has to be solved to find $\{\widehat{\boldsymbol{x}}^{n+1}, \widehat{\boldsymbol{v}}^{n+1}\}$. The non-linear equations are solved using an iterative Newton Method. In most cases full convergence is obtained in 3 or 4 iterations. In next section we present some obtained numerical simulations.

4 NUMERICAL SIMULATIONS

To perform the numerical simulations described in this section, we used the code `MulPhys` Limache (2007). The code contains a module called `MulPhys-FEM` which produces numerical simulations based on an advanced FEM formulation for large deformations. The advanced Finite Volume formulation discussed in this paper has been implemented and coupled into the main program in another module called `MulPhys-FV`.

4.1 Flexible Pendular Bar

In this numerical test, we run the case of a pendulum made of an hyperelastic rectangular bar. The bar is fixed to the wall only in its left lower corner. At time t=0, the bar is released and starts falling and rotating due to its own weight. As a consequence, moves in a pendular motion, as shown in figure 3. On the left side of the figure, the results corresponding to the use of a FEM-formulation are shown, and on the right, the results obtained using the developed FV-Formulation are displayed. In figures 4-5 the corresponding displacements of the free extremum of the bar are shown as a function of time. Note that the FV formulation gives completely
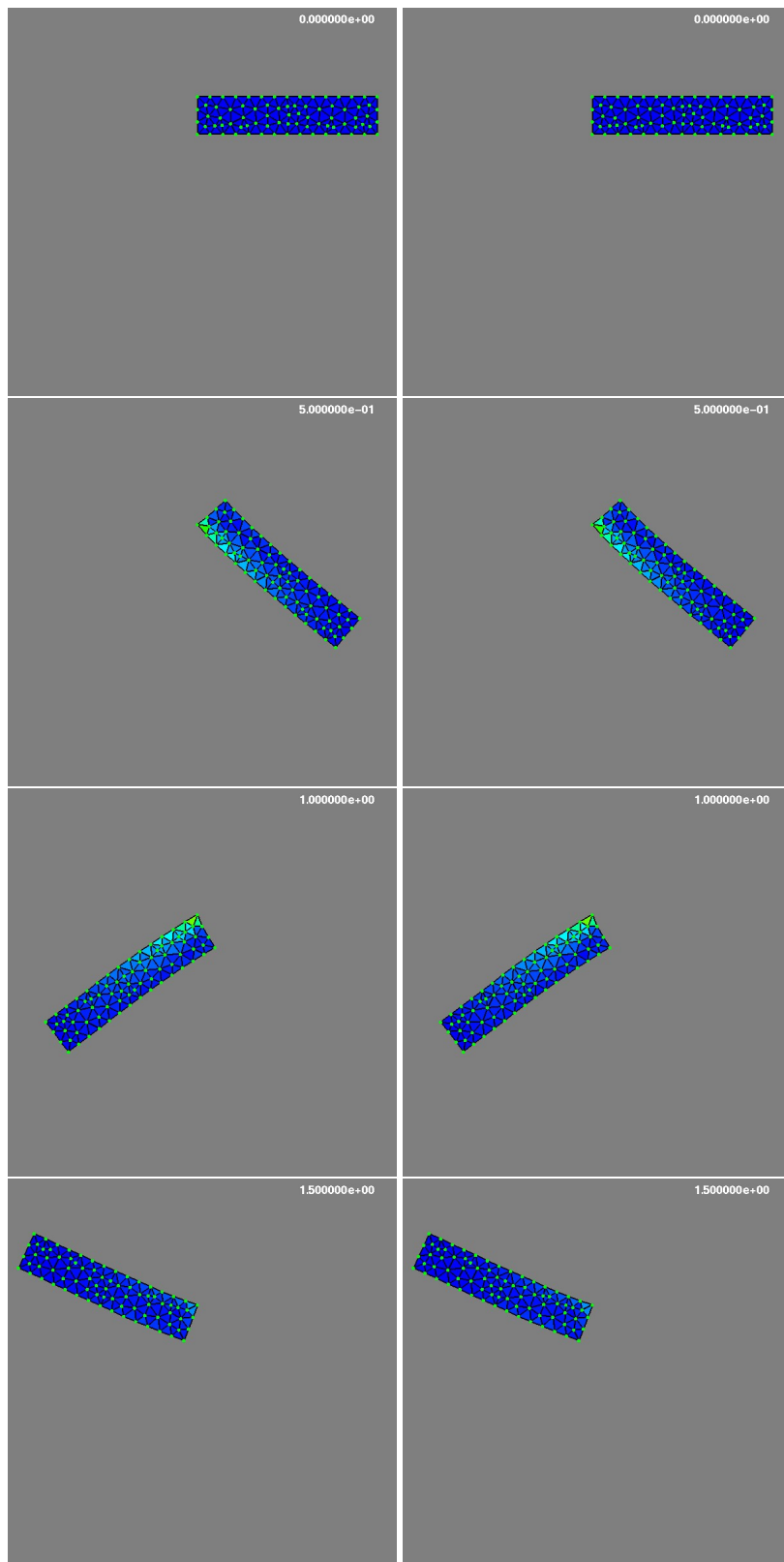
Figure 3: Numerical Simulations of a Pendulum made of a flexible hyperelastic bar. On the left the FEM formulation, and on the right, the Finite Volume formulation.
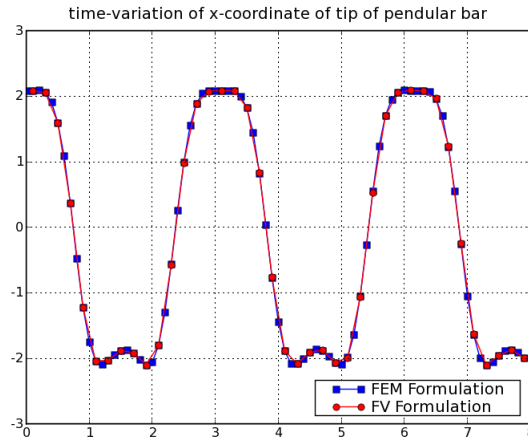
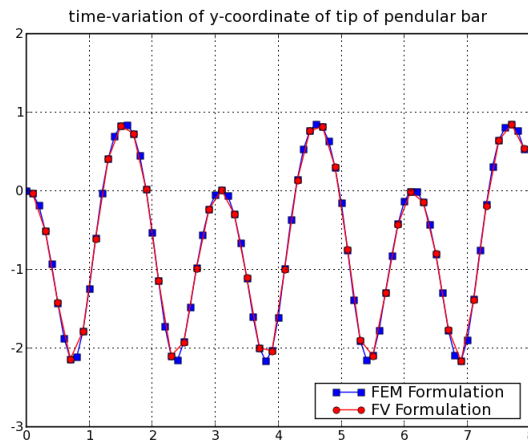Figure 4: time-variation in the x-direction of the free extremun of the pendular bar

Figure 5: time-variation in the y-direction of the free extremun of the pendular bar

similar results to the FEM formulation. Note that both formulations do not seem to produce any appreciable numerical dissipation and they predict the same frequency of oscillations

4.2 Clamped Bar subject to a constant load

In this numerical test, we run the case of a rectangular bar made of a flexible hyperelastic material that is clamped to the wall on its left extremum. At time t=0, the bar is released and subject to a constant vertical load, on the node that corresponds to the botton right corner of the bar. As a consequence of the load the bar deflects downwards and starts an oscillatory motion, as shown in figure 6. On the left side of the figure, the results corresponding to the use of a FEM-formulation are shown, and on the right are shown the results obtained using the developed FV-Formulation.

In figures 7-8 the corresponding displacements of the right extremum of the bar are shown as a function of time. Note that both formulations predict the same dynamical behavior, matching in amplitude and frequency of oscillation. Note that the numerical simulations produced by `MulPhys-FEM` and `MulPhys-FV` do not produce any appreciable numerical dissipation, this is extremely important because hyperelastic materials conserve energy. In the same figures, a
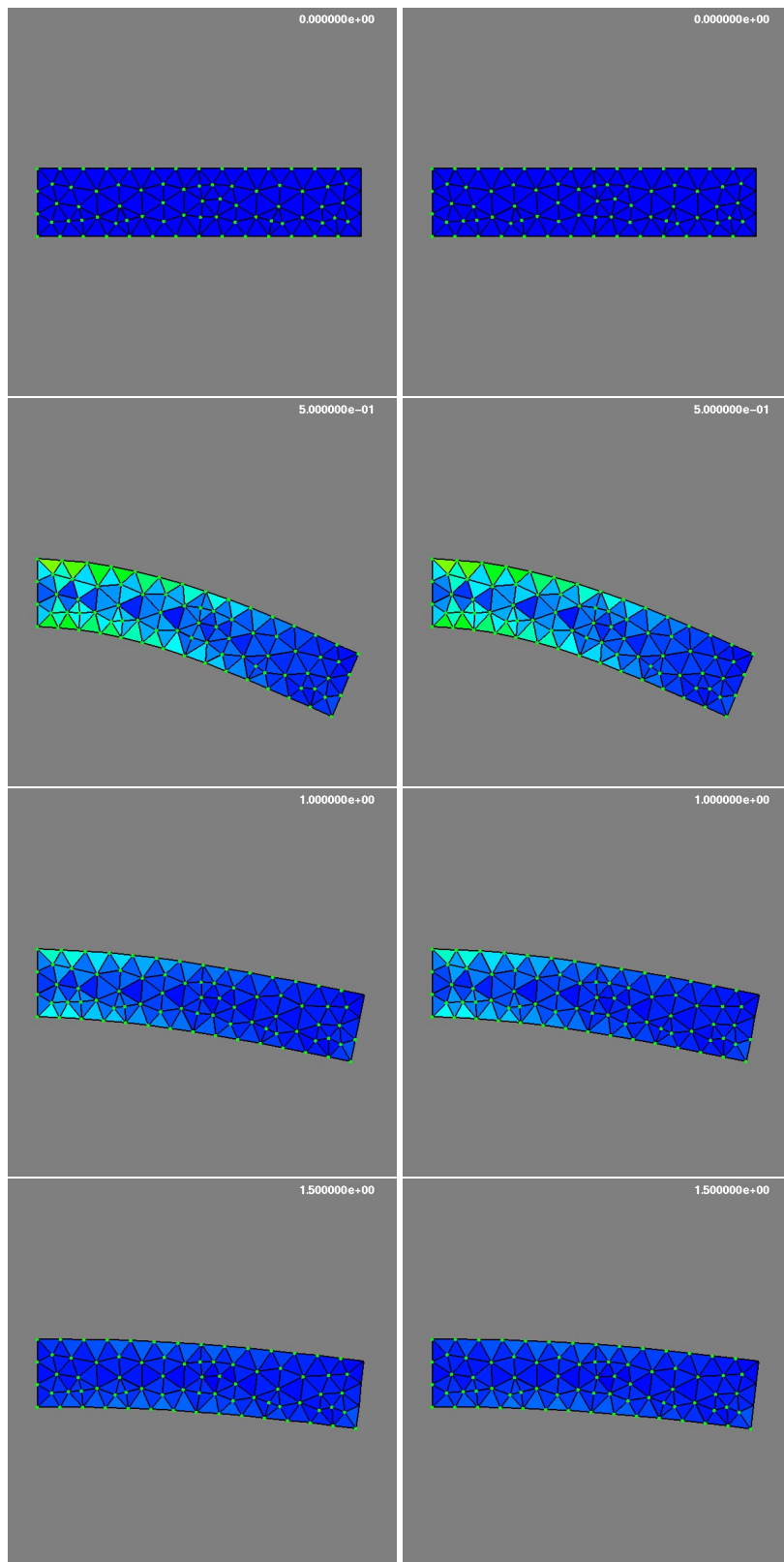
836

Figure 6: Numerical Simulations of a clamped bar made of a flexible hyperelastic material. On the left the FEM formulation, and on the right the Finite Volume formulation
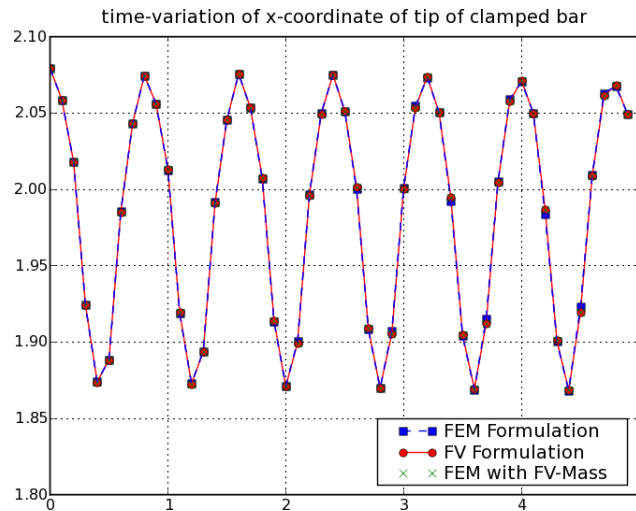
Figure 7: time-variation in the x-direction of the free extremun of clamped bar

third simulation is displayed containing the numerical results when the standard FEM formulation is modified to have the *Mass Matrix* of the FV formulation. We see again a excellent matching in the obtained results.

4.3 Deformable Planet in orbit around a gravitational field

In this numerical test, we run the case of a circular planet made of a flexible hyperelastic material that is put into orbit around a gravitational field. At time t=0, the planet is put in an initial condition: it is located along the y-axis and an appropriate horizontal velocity is given to it, after that time the planet moves freely while being attracted by the gravitational field, as shown in figure 9. On the left side of the figure, the results corresponding to the FEM-formulation are shown, and on the right the results obtained using the developed FV-Formulation are displayed. Observe that again both formulations give almost the same result.

In figures 10-11 the corresponding displacements of the planet are shown as a function of time. In figure 12 the planet's trajectory around the gravitational field is shown. From these figures we clearly see that the FV formulation predicts the same results than the FEM formulation

5   CONCLUSIONS

Our first attempt in the development of Finite Volume Formulations for Computational Solid Mechanics has been succesful. The results presented in this article are promising and shown that it is possible to develop robust and stable FVM formulations not only for CFD but also for CSD. Further research is in course to investigate more properties of FV formulations. The FV formulation discussed in this paper incorporates all the features that are necessary for performing large-deformations, large rotations and large displacements. Those features were traditionally only accesible via FEM, now, FEM has a new competitor to dispute its supremacy in CSD.
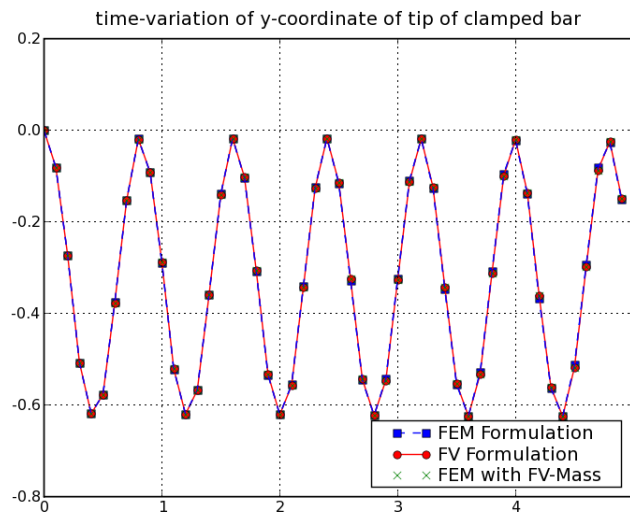
Figure 8: time-variation in the y-direction of the free extremun of clamped bar

REFERENCES

ABAQUS. *http://www.abaqus.com*. ABAQUS, 2007.

Atwood C.A. Navier-stokes simulations of unsteady transonic flow phenomena. *NASA-TM-103962*, 1992.

Bergamaschi L., Mantica S., and Manzini. G. A mixed finite element-finite volume formulation of the black-oil model. *SIAM J. Sci. Comput.*, 20:970–997, 1999.

Biedron R.T. Simulation of unsteady flows using an unstructured navier-stokes solver on moving and stationary grids. *AIAA Paper 2005-5093*, 2005.

Bijelonja I., Demirdzic I., and Muzaferija S. A finite volume method for incompressible linear elasticity. *, Computer Methods in Applied Mechanics and Engineering*, 2006.

CFX. *http://www-waterloo.ansys.com/cfx/*. CFX, 2007.

Chandio M., Sujatha K., and Webster M.F. Consistent hybrid finite volume/element formulations: Model and complex viscoelastic flows. *Internat. J. Numer. Methods Engrg.*, 45:945–971, 2004.

Cheatwood F. and Gnoffo P. User's manual for the langley aerothermodynamic upwind relaxation algorithm (laura). *NASA TM-4674*, 1996.

Chen J., Wu C., and You Y. A stabilized conforming nodal integration for galerkin mesh-free methods. *Internat. J. Numer. Methods Engrg.*, 50:435–466, 2001.

Chung E. and Zou J. A finite volume method for maxwell's equations with discontinuous physical coefficients. *International J. Appl. Math.*, 7:201–223, 2001.

Cook R., Malkus D., and Plesha M. *Concepts and Applications of Finite Element Analysis*. Wiley, 2001.

FEATFLOW. *http://www.featflow.de*. FEATFLOW, 2007.

Frink N. and Pirzadeh S. Tetrahedral finite-volume solutions to the navier-stokes equations on complex configurations. *NASA/TM-1998-208961*, 1998.

Geiger S., Roberts S., Matthai S.K., and Zoppou C. Combining finite volume and finite element
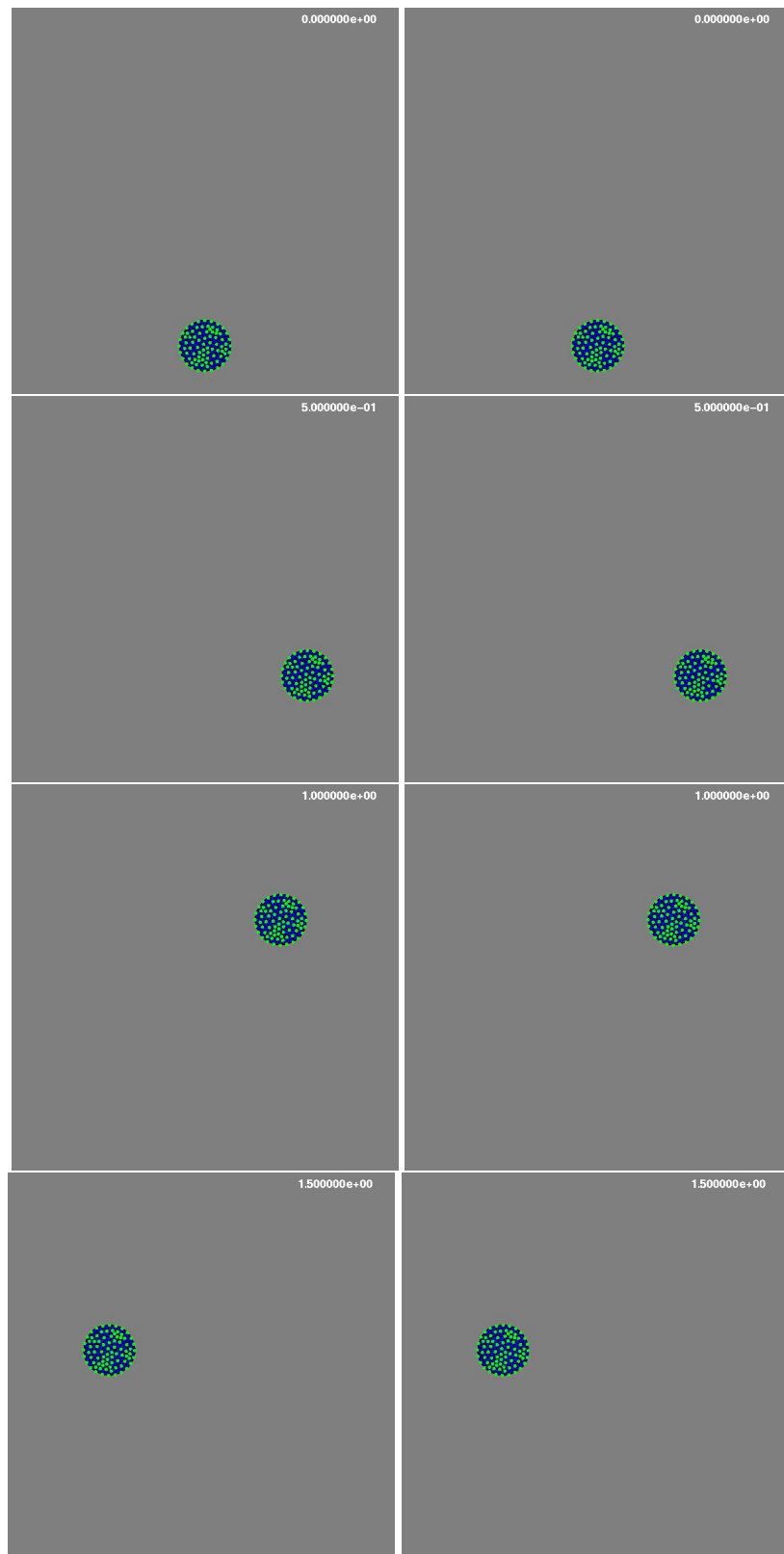
Figure 9: Numerical Simulations of the motion of a deformable circular planet made of an hyperelastic material around a gravitational field. On the left the FEM formulation, and on the right the Finite Volume formulation
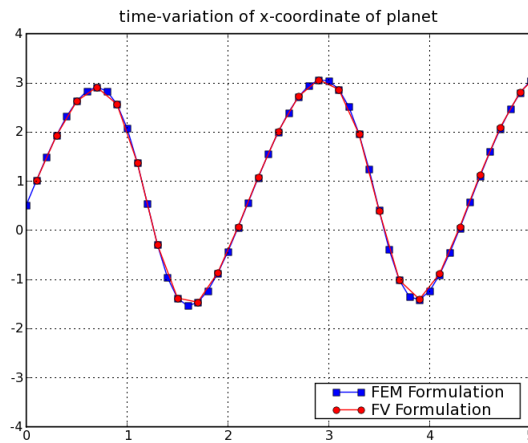
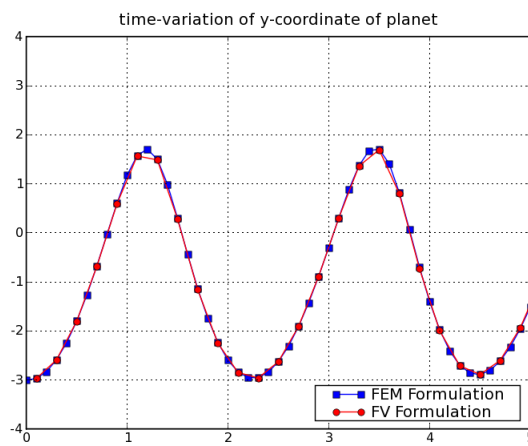Figure 10: Displacement of the planet in the y-direction as a function of time

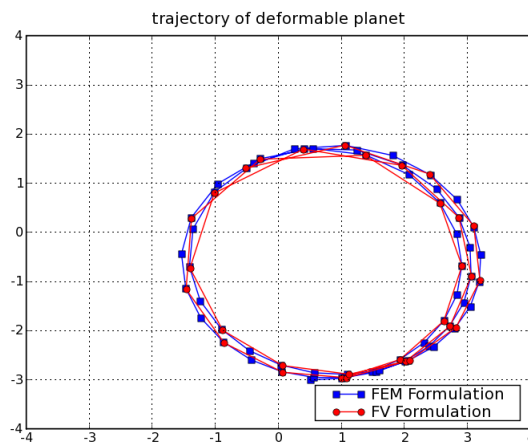Figure 11: Displacement of the planet in the y-direction as a function of time

Figure 12: Planet's trajectory around the gravitational field located at the origin

methods to simulate fluid flow in geologic media. *ANZIAM J.*, 44-E:C180–C201, 2003.

Gurtin M. *An Introduction to Continuum Mechanics*, volume Mathematics in Science and Engineering, 158. Academic Press, 1981.

Howell B.P. and Ball G.J. A free-lagrange augmented godunov method for the simulation of elastic-plastic solids. *Journal of Computational Physics*, 175:128–167, 2002.

Hubbard M. and Roe P. Multidimensional upwind fluctuation distribution schemes for scalar time dependent problems. *Int. J. Numer. Methods Fluids*, 33:711 – 736, 2000.

Hughes T. *The Finite Element Method ; Linear Static and Dynamic Finite Element Analysis*. Dover Publishers, 2000.

Johnson C. *Numerical Solutions of Partial Differential Equations by FEM*. Studentliteratur, 1987.

Lax P. and Wendroff B. Systems of conservation laws. *Comm. Pure. Appl. Math.*, 13:217–237, 1960.

Leer B.V. Flux vector splitting for the euler equations. *In E. Krause, editor, Proceedings of the 8th International Conference on Numerical Methods in Fluid Dynamics*, pages 507–512, 1982.

Leveque R. *Finite Volume Methods for Hyperbolic Problems*. Cambridge University Press, 2002.

Limache A. and Cliff E. Aerodynamic sensitivity theory for rotary stability derivatives. *AIAA-Journal of Aircraft*, 37:676–683, 2000.

Limache A.C. *MulPhys, A Computational Tool for Multi-Physics*. CIMEC, 2007. Http://www.cimec.org.ar/alimache/.

Matallah H., Townsend P., and Webster M.F. Recovery and stress-splitting schemes for viscoelastic flows. *J. Non-Newt. Fluid Mech.*, 75:139–166, 1998.

Ogden R.W. *Non–Linear Elastic Deformations*. Series in mathematics and its applications. Ellis Horwood Limited, 1984.

Onate E. *Cálculo de Estructuras por el Método de Elementos Finitos*. CIMNE, 1995.

Ottosen N. and Ristinmaa M. *The Mechanics of Constitutive Modeling*. Elsevier, 2005.

PETScFEM. *http://www.cimec.org.ar/petscfem*. CIMEC, 2007.

Ramesh B. and Maniatty A.M. Stabilized finite element formulation for elastic-plastic finite deformations. *Computer Methods in Applied Mechanics and Engineering*, 194:775–800, 2005.

Rente C. and Oliveira P. Extension of a finite volume method in solid stress analysis to cater for non-linear elastoplastic effects. *EM2000 Fourteenth Engineering Mechanics Conference*, 2000.

Rumsey C. and Vatsa V. A comparison of the predictive capabilities of several turbulence models using upwind and centered-difference computer codes. *AIAA Paper 93-0192*, 1993.

Slone A.K., Bailey C., and Cross M. Dynamic solid mechanics using finite volume methods. *Applied Mathematical Modelling*, 27:69–87, 2003.

Souli M., Ouahsine A., and Lewin L. Ale formulation for fluid-structure interaction problems. *Computer Methods in Applied Mechanics and Engineering*, 190:659–675, 2000.

Szabo B. and Babuska I. *Finite Element Analysis*. Wiley, 1991.

Taylor G., Bailey C., and Cross M. Computational solid mechanics using a vertex-based finite volume method. *In F. Benkhaldoun and D. Hanel, editors, Finite Volumes for Complex Applications II: Problems and Perspectives*, pages 507–515, 1999a.

Taylor G.A., Hughes M., Strusevich N., and Pericleous K. Finite volume methods applied to the computational modelling of welding phenomena. *Second International Conference on*

CFD in the Minerals and Process Industries CSIRO, 1999b.

Teran J., Blemker S., Hing V.N.T., and Fedkiw R. Finite volume methods for the simulation of skeletal muscle. *Eurographics/SIGGRAPH Symposium on Computer Animation*, 2003.

Versteeg H. and Malalasekera W. *An Introduction to Computational Fluid Dynamics, The Finite Volume Method*. Longman Scientific & Technical, 1995.

Wheel M. A mixed finite volume formulation for determining the small strain deformation of incompressible materials. *Int. Journal for Num. Methods in Engn.*, 44:1843–1861, 1999.

Zarrabi K. and Basu A. A finite volume element formulation for solution of elastic axisymmetric pressurized components. *International Journal of Pressure Vessels and Piping*, 77:479–484, 2000.

Zienkiewicz O. and Taylor R. *The finite element method*, volume I-III. McGraw Hill, 1991.